Evaluation of PolInSAR Observables for Crop-Type Mapping Using Bistatic TanDEM-X Data

Noelia Romero-Puig, *Graduate Student Member, IEEE*, Juan M. Lopez-Sanchez, *Senior Member, IEEE*, Mario Busquier, *Student Member, IEEE*

***Abstract*—The contribution of Polarimetric SAR Interferometry (PolInSAR) observables to crop-type classification is investigated in this letter. The focus is set on characteristic parameters of the Coherence Region (CoRe), i.e. the representation in the polar plot of the PolInSAR data. For this purpose, time series of dual-pol HH-VV single-pass TanDEM-X bistatic data acquired over an agricultural area in Spain are exploited. In the experiment, up to 13 different crop types are evaluated. Crop classification is performed by means of the well-known Random Forest algorithm. The retrieved accuracy metrics highlight the potential of the evaluated PolInSAR descriptors for this application. Some PolInSAR features have proven to be enough representative of the scene, such as the Trace Coherence, which yields a classification accuracy of 75% and 87% at pixel and field level, respectively, on its own. Using all the PolInSAR parameters jointly as input features, classification reaches around 90% and 94% accuracy at pixel and field level, respectively. However, there are some PolInSAR feature subsets, e.g. the coherence measured at the Pauli channels or the foci of the ellipse which represents the CoRe, which yield accuracy levels very close to these maxima. These results demonstrate the suitability of the PolInSAR parameters for crop-type classification. Results are further improved when both polarimetric and PolInSAR features are combined, reaching 94% and 96% accuracy at pixel and field level, respectively.**

***Index terms*—** Agriculture, classification, crop-type, PolInSAR, TanDEM-X, Trace Coherence.

I. Introduction

CROP-TYPE classification maps are today valuable products for both agricultural managers and paying agencies, which exploit them for a broad range of applications, from prediction of harvest yield to estimation of disaster compensation or the design of biodiversity preservation strategies, among others. In this context, timely and precise crop monitoring, as offered by the Synthetic Aperture Radar (SAR) systems, is crucial to reduce the cost of physical field inspections and to advance towards operational level applications [1].

Time series of dual polarimetric HH-VV SAR data acquired by the single-pass bistatic TanDEM-X [2] system during the Science Phase in 2015 were gathered using large spatial baselines and in absence of temporal decorrelation. These are key characteristics for crop monitoring by means of spaceborne Polarimetric SAR Interferometry (PolInSAR) [3]. The potential of such a data set has been demonstrated in the past for the quantitative estimation of crop parameters, with focus on the vegetation height [4].

Regarding crop classification, previous experiments exploiting X-band SAR data, either from the TerraSAR-X satellite alone or with the TanDEM-X system, have obtained successful results employing different polarimetric SAR (PolSAR) descriptors [5], [6], and also by means of interferometric SAR (InSAR) products [7], [8]. However, the information provided by the combination of both polarimetric and interferometric observables for this purpose remains unexplored.

In this work, we propose to investigate the added value of PolInSAR descriptors for crop-type classification. In particular, parameters derived from the Coherence Region (CoRe) [9], as the representation in the complex plane of the PolInSAR data, are employed as input features for classification. In addition, the operator known as Trace Coherence (TrCoh) [10], which has proven a valuable parameter for crop height estimation [11], is tested. By exploiting the geometrical representation of the CoRe, which is an ellipse for dual-pol data, as those provided by the TanDEM-X system, additional observables which provide further insights into the physical scene can be retrieved. The crop classification accuracy achieved with these PolInSAR parameters, together with the coherence observed at the lexicographic and Pauli basis, is analysed and assessed.

II. Polarimetric SAR Interferometry

PolInSAR [3] systems combine information provided by sets of images acquired at multiple polarisations. Considering dual-pol HH-VV TanDEM-X bistatic data [2], each acquisition can be expressed as a scattering vector $\vec{k}_n = [S^n_{\text{HH}},\ S^n_{\text{VV}}]^T$, $n = 1, 2$, where S^n_{PP} represents the complex scattering amplitude at the n-th end of the spatial baseline.

The basic PolInSAR observable used to describe all scatterers present in the observed target (i.e. image pixel) is the covariance $[C]$ matrix (in the lexicographic basis):

$$[C] = \begin{bmatrix} \langle \vec{k}_1 \cdot \vec{k}_1^{*T} \rangle & \langle \vec{k}_1 \cdot \vec{k}_2^{*T} \rangle \\ \langle \vec{k}_2 \cdot \vec{k}_1^{*T} \rangle & \langle \vec{k}_2 \cdot \vec{k}_2^{*T} \rangle \end{bmatrix} = \begin{bmatrix} [C_{11}] & [\Omega_{12}] \\ [\Omega_{12}]^{*T} & [C_{22}] \end{bmatrix}, \quad (1)$$

where superscript $*T$ denotes conjugate transpose, and $\langle \cdot \rangle$ spatial averaging. $[C_{11}]$ and $[C_{22}]$ are 2×2 matrices containing polarimetric information, while $[\Omega_{12}]$ is a 2×2 matrix containing both polarimetric and interferometric information.

This work was supported by the Spanish Ministry of Science and Innovation, the State Agency of Research (AEI) and the European Funds for Regional Development (EFRD) under Project PID2020-117303GB-C22. Mario Busquier received a grant from the University of Alicante [UAFPU20-08].

Noelia Romero-Puig was with the Institute for Computer Research (IUII), University of Alicante, 03080 Alicante, Spain. She is now with the Microwaves and Radar Institute, German Aerospace Center (DLR), 82234 Wessling, Germany (e-mail: noelia.romeropuig@dlr.de).

Juan M. Lopez-Sanchez and Mario Busquier are with the Institute for Computer Research (IUII), University of Alicante, 03080 Alicante, Spain (e-mail: juanma-lopez@ieee.org, mario.busquier@ua.es).

The projection of the scattering vector $\vec{k}_n$ on unitary complex vectors $\vec{\omega}$, which specify the selected polarimetric combination, yields $S_n(\vec{\omega}) = \vec{\omega}^{*T} \cdot \vec{k}_n$ [3]. The interferometric combination of the scalars $S_n(\vec{\omega})$ results in the PolInSAR coherence:

$$\gamma(\vec{\omega}) = \frac{\vec{\omega}^{*T}[\Omega_{12}]\vec{\omega}}{\sqrt{(\vec{\omega}^{*T}[C_{11}]\vec{\omega})(\vec{\omega}^{*T}[C_{22}]\vec{\omega})}}. \quad (2)$$

The CoRe [9] is the geometrical representation in the complex plane of all possible PolInSAR coherences varying with the projection vector: $\{\gamma(\vec{\omega}), \vec{\omega} \in \mathbb{C}^2, \|\vec{\omega}\| = 1\}$. A common technique to derive mathematical properties from the CoRe consists in employing a simplified PolInSAR matrix $[A]$ [12, eq. (6.33)], defined as

$$[A] = \sqrt{[C_a]^{-1}}[\Omega_{12}]\sqrt{[C_a]^{-1}}, \text{ with } [C_a] = \frac{[C_{11}] + [C_{22}]}{2}. \quad (3)$$

In the case of dual-pol data, $[A]$ is a 2×2 matrix. The field of values of any 2×2 matrix is an ellipse [13]. From $[A]$ (3), it is possible to derive the characteristic parameters of the CoRe by means of a Schur decomposition (see [12, eq. (6.31)])

$$[A] = \begin{bmatrix} a_{11} & a_{12} \\ a_{21} & a_{22} \end{bmatrix} \Rightarrow [A] = [U_2]^{*T} \begin{bmatrix} \lambda_1 & \delta \\ 0 & \lambda_2 \end{bmatrix} [U_2], \quad (4)$$

where

$$\begin{aligned} 2a &= \sqrt{|\lambda_1 - \lambda_2|^2 + |\delta|^2}, \\ 2b &= |\delta|, \\ g_m &= \frac{1}{2}(\lambda_1 + \lambda_2). \end{aligned} \quad (5)$$

In (5), $2a$ and $2b$ are the major and minor axis, g_m is the ellipse centre (i.e. mean coherence), and λ_1 and λ_2 are the foci of the ellipse.

Another parameter of interest of the CoRe is the operator TrCoh [10], defined as:

$$\gamma_{\text{tr}} = \frac{\text{Trace}([\Omega_{12}])}{\sqrt{\text{Trace}([C_{11}])\text{Trace}([C_{22}])}}. \quad (6)$$

As an approximation of the centre of mass of the CoRe, the TrCoh provides a significant representation of the observed target which is not associated with any specific scattering mechanism. These properties make it suitable for crop parameter estimation by means of PolInSAR [11].

In contrast to the TrCoh, the coherence extrema $\gamma(\vec{\omega}_{\text{min}})$ and $\gamma(\vec{\omega}_{\text{max}})$ are associated with the scattering mechanisms which maximise the phase centre separation. Physically, these are the coherences furthest and closest to the topographic phase. Hence, they are commonly employed for its estimation by using a line fit [3], [12].

A representation of the border of the CoRe, together with its characteristic parameters, is shown in Fig. 1. The CoRes of the four selected crop types corroborate that the PolInSAR signature of each pixel is different according to the specific crop structural (e.g. height, density) and dielectric (e.g. water content) properties.

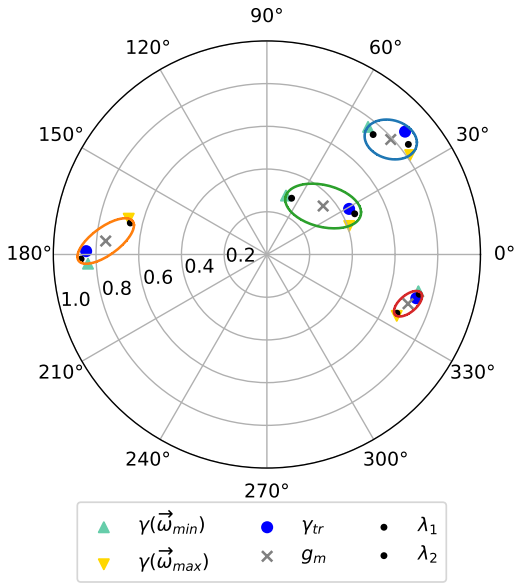

Fig. 1. Unit circle on the complex plane representing the characteristic parameters of the CoRe of 4 pixels corresponding to different crop types. Colours represent the border of the CoRe (i.e. ellipse): alfalfa (blue), sugar beet (orange), maize (green) and wheat (red). Data correspond to an acquisition obtained on 18 July 2015 with the TanDEM-X bistatic system.

III. Test Site and Data Set

An agricultural area in Sevilla, SW of Spain (37.1 N, 6.15 W), is selected for crop-type classification. As shown in Fig. 2, we can divide the test site into two large areas: a rice area located in the NW (in light blue), and an area known as the BXII Sector, where different crop types are cultivated. A total of 13 crop classes are considered in the experiment.

In this work, we have exploited 9 dual-pol HH-VV TanDEM-X [2] bistatic acquisitions taken from 4 June to 31 August 2015. The available time series corresponds to an incidence angle of 22.7°and is characterised by large spatial baselines, i.e. vertical wavenumber κ_Z = 2.48 rad/m, and small heights of ambiguity, i.e. 2.53 m. The observation interval ranges 3 months and covers different crop phenological stages, including seeding, growing, harvesting and post harvest.

The starting point of the SAR data processing are the standard Coregistered Single-Look Slant-range Complex (CoSSC) TanDEM-X products. The spatial resolution of the images is 6.6 m in azimuth and 3.1 m in range, whereas the pixel size is 2.4 m in both coordinates. First, range spectral filtering is applied to compensate for the geometrical decorrelation. Next, multi-looking is carried out employing a 21×21 boxcar filter. After the multi-looking, the spatial resolution is around 50 m in both directions. Prior to the interferogram formation, flat Earth and topographic phase contributions are removed, thus yielding differential interferograms. In the end, the products are geocoded.

IV. Crop Classification Method

Crop-type mapping is carried out by means of the Random Forest (RF) [14] classifier implemented in Python. The number of decision tree estimators is set to 1000, and the rest of

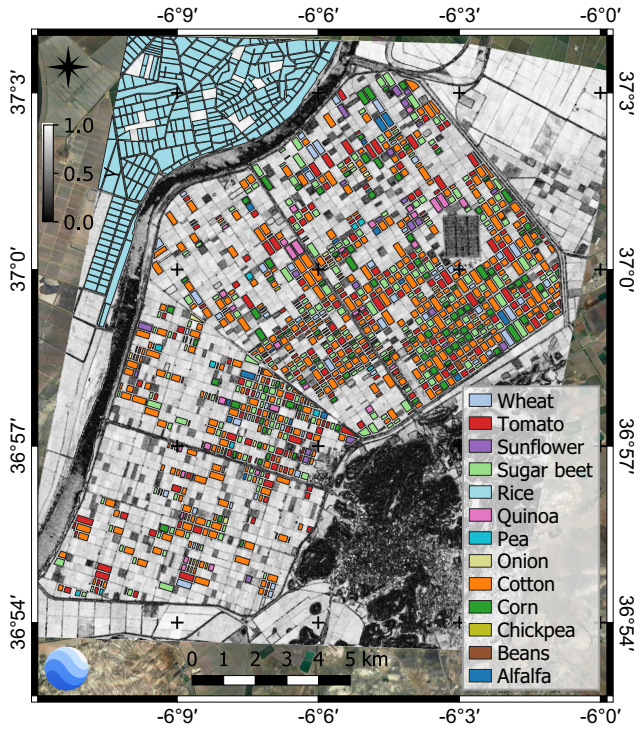

Fig. 2. Study area located in Sevilla, Spain. The coherence amplitude of the HH channel acquired on 26 June 2015 with the TanDEM-X system is presented. The different crop classes available are specified.

hyper-parameters are set to their default values. The number of features considered by each decision tree when dividing a node is the square root of the total number of features.

The large 21 $\times$ 21 kernel size of the boxcar filtering, suitable for PolInSAR data, yields correlated neighbouring pixels. Hence, in first place, for each crop type, 50% of the fields are selected for training and the remaining 50% for testing. Next, similarly to the method described in [8], a balanced training strategy is achieved by randomly selecting the same number of pixels per class. This is constrained to the class with the least number, for which all pixels of the training set are considered. In third place, the evaluation step is carried out including all pixels of the initial testing set. At last, the described training and testing steps are repeated 10 times and the resulting accuracy metrics are averaged. This avoids possible peculiarities of the initial (random) training-testing fields split and it also ensures stable results.

Fig. 3 represents the temporal evolution of the PolInSAR observables corresponding to characteristic parameters of the CoRe, as defined in Section II. For the sake of simplicity, 4 (out of 13) crop types with different characteristics are selected, i.e. alfalfa, sugar beet, maize and wheat. The time series of the rest of available crops is included in the supplementary material. The first three parameters (row 1) are related to the coherence extrema and the phase difference between these two. The remaining parameters (rows 2 and 3) correspond to the TrCoh and those related purely to the geometrical shape of the CoRe, i.e. an ellipse for dual-pol data. The time series of all the crop types are included in the supplementary material.

Attending to the evolution of these parameters, the most representative features (i.e. with greatest dynamic range) are selected and grouped for crop classification. This includes: the TrCoh alone, the ellipse axes, the ellipse foci, the coherence extrema, and all the above together. In addition to these parameters, the coherence observed at the polarisation channels in the lexicographic basis, i.e γ_{HH} and γ_{VV}, and in the Pauli basis, i.e γ_{P1} and γ_{P2}, where P1 = HH + VV, P2 = HH $-$ VV, constitute a second set of input features. Then, in another test, all the described PolInSAR parameters are employed jointly for crop classification.

Finally, to further assess the added value of these PolInSAR descriptors for crop-type mapping, the analysis is completed by considering purely polarimetric features. This includes the backscattering power at the linear and Pauli channels, as well as the corresponding polarimetric correlation (as defined in [8, eq. (2)]) and phase, i.e. ρ_{HHVV}, ϕ_{HHVV}, ρ_{P1P2}, ϕ_{P1P2}.

The classification results are evaluated in two ways: at pixel level and at field level. In the first case, each pixel is assigned a crop class. In the second case, each field is classified according to the mode (most frequent value) of all the classes assigned to the pixels composing the field. In addition, the importance of the individual features employed in the classification experiments was retrieved. The most representative cases are shown as figures in the supplementary material, but they are commented in the Results section.

V. Results

A. Results with PolInSAR Observables

A straightforward evaluation of the suitability of the PolInSAR features for crop classification based on the Overall Accuracy (OA) is presented in Table I. **Coh Min** and **Coh Max** refer to the coherences with minimum and maximum phase, **F1** and **F2** to the ellipse's foci. **Set 1** includes all the previous features: TrCoh, axes and foci of the ellipse, and the coherence extrema.

TABLE I
Classification scores obtained with PolInSAR observables.

Features	OA (%)	
	Pixel level	Field level
Major axis + Minor axis	64.19	82.89
TrCoh	74.58	87.44
F1 + F2	85.51	92.82
Coh Min Pha + Coh Max Pha	80.54	91.13
Set 1	88.57	93.97
Coh HH + Coh VV	80.26	88.47
Coh P1 + Coh P2	88.67	93.63
All PolInSAR features	89.05	94.00

At first glance, Table I shows that the OA obtained at pixel level is, in most cases, above 80%. Only when parameters related strictly to the geometrical shape of the CoRe, not its position, like the ellipse axes employed alone, the OA is worse, i.e. 64.19%. With the rest of CoRe parameters (originally complex numbers), OA levels around 75% and beyond are retrieved. This is achieved even when exploiting the TrCoh alone, with an OA = 74.58%. Indeed, this result

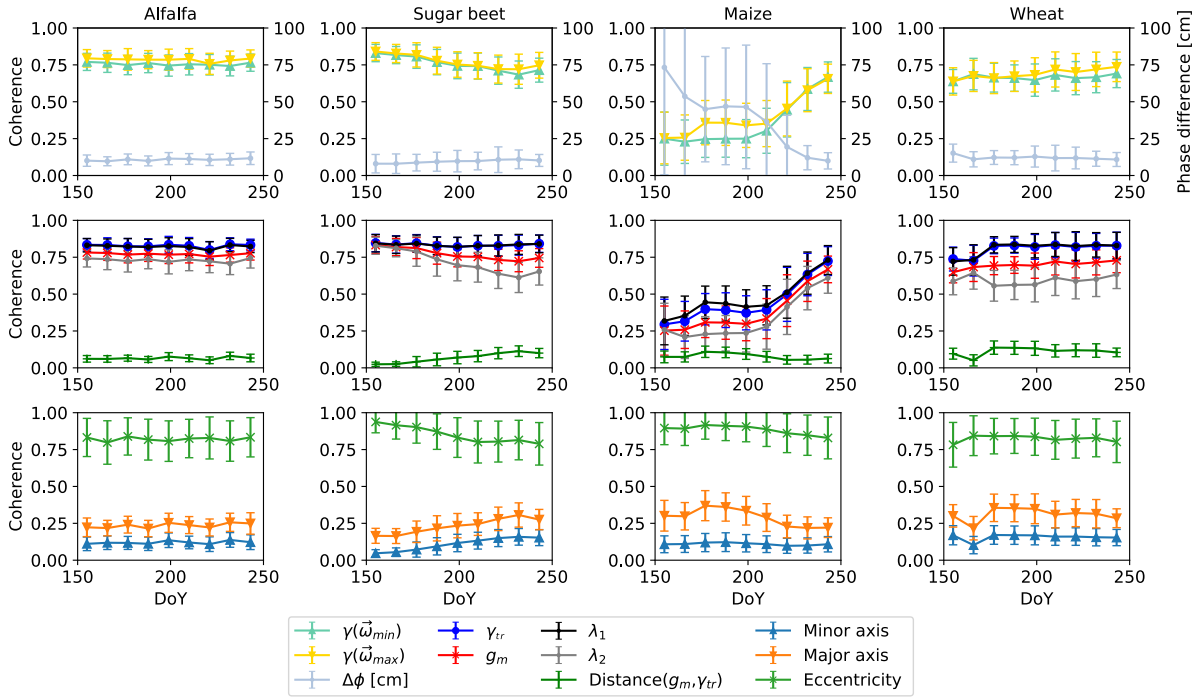

Fig. 3. Time series of PolInSAR observables, i.e. characteristic parameters of the CoRe, for 4 selected crop types: alfalfa, sugar beet, maize and wheat. Average values of all the available pixels for each crop type (including training and testing samples) are considered, and error bars denote $\pm$ standard deviation.

demonstrates the strong physical meaning of this parameter, as most representative of the natural observed scene.

Observations derived from the results evaluated at pixel level are corroborated at field level, where the final OA improves. Table I reveals a high accuracy in all the experiments. The lowest OA is around 83% for the case in which the ellipse axes are used for classification. However, for the remaining feature sets evaluated, OA levels are either above 90% or very close to it: 87.44% when considering the TrCoh alone for classification, and 88.47% employing $\gamma_{\mathrm{HH}} + \gamma_{\mathrm{VV}}$.

In both assessments, at pixel and at field level, a common behaviour is that, as expected, the highest classifications scores are reached when combining different PolInSAR features. Thus, accuracies around 89-94% at pixel and field level, respectively, are obtained when including the TrCoh, the ellipse axes and foci and the coherence extrema together for classification (**Set 1** in Table I), and also when considering all these features. In particular, when evaluating the **Set 1** of features, the RF algorithm shows that the parameter with the highest importance in the classification is the TrCoh (i.e. with an importance of 0.04). This justifies the high classification accuracy obtained when using this feature alone. Nevertheless, when including all the parameters, the highest importance for the classification lies on γ_{P2} and λ_2 with a 0.03, followed closely by the γ_{tr} with a 0.02. In all cases, features with the highest importance correspond to those at the beginning of the growth cycle, either at June 4 or 15, while features with the least (or null) importance correspond to the minor axis retrieved close to the end of the campaign.

In addition, it is worth noting that feature subsets including only $\lambda_1 + \lambda_2$, and only $\gamma_{\mathrm{P1}} + \gamma_{\mathrm{P2}}$, reach OA values very close to the maxima, i.e. around 86-93% at pixel and field level in the first case, and almost 89-94% in the second case, respectively.

B. Comparison with PolSAR Observables

The assessment of the contribution of the PolInSAR descriptors with respect to purely PolSAR ones is completed with the classification results presented in Table II. **HH**, **VV**, **P1** and **P2** refer to the backscattering coefficients of the corresponding polarization channels in linear and Pauli basis; **Corr HHVV**, **Pha HHVV** and **Corr P1P2**, **Pha P1P2** denote polarimetric correlation and phase between HH and VV, and between P1 and P2, respectively.

Notably, classifying employing the backscatter coefficients alone already provides high accurate results, with an OA at pixel and field level of 86.95-90.33% and 92.55-94.72% at the linear and Pauli channels, respectively. This accuracy improves when including the polarimetric correlation and the interferometric coherence magnitudes. However, as expected, the OA does not improve when considering the polarimetric phase. This is corroborated when inspecting the importance results, which reveal the lack of useful information for classification purposes of this parameter, i.e. importance levels of 0.01.

The best classification results are obtained when employing the backscatter and polarimetric correlation magnitudes with some PolInSAR observables. For instance, Table II shows that at the Pauli channels, OA levels around 94-96% at pixel and field level are reached when adding either the foci of the ellipse, the TrCoh or the coherence extrema. Such accuracy scores are only reached when including several PolInSAR observables (see Table I), as with the **Set 1** (i.e. 88.57-93.97%), the coherence at the Pauli channels (i.e. 88.67-

TABLE II
CLASSIFICATION SCORES OBTAINED WITH OTHER SAR OBSERVABLES.

Features	OA (%) Pixel level	OA (%) Field level
HH + VV	86.95	90.33
HH + VV + Coh HHVV	92.45	94.38
HH + VV + Coh HHVV + Pha HHVV	92.44	94.40
P1 + P2	92.55	94.72
P1 + P2 + Corr P1P2	93.11	95.22
P1 + P2 + Corr P1P2 + Pha P1P2	92.44	94.40
HH + VV + Corr HHVV + Coh HH + Coh VV	93.54	95.10
P1 + P2 + Corr P1P2 + Coh P1 + Coh P2	94.30	95.54
HH + VV + Corr HHVV + F1 + F2	93.71	95.38
P1 + P2 + Corr P1P2 + F1 + F2	94.30	96.04
HH + VV + Corr HHVV + TrCoh	93.51	95.04
HH + VV + Corr HHVV + Coh Min + Coh Max	93.89	95.46
P1 + P2 + Corr P1P2 + TrCoh	94.20	95.93
P1 + P2 + Corr P1P2 + Coh Min + Coh Max	94.30	96.06
PolSAR + PolInSAR	94.11	95.90

93.63%), and all the PolInSAR features together (i.e. 89.05-94%). However, as the last test in Table II demonstrates, this maximum accuracy is not surpassed when adding jointly the set of PolInSAR and PolSAR features: OA = 94.11-95.90%. The importance of the different features indicates that the most determining descriptor for crop-type classification is the backscattering coefficient at P2, i.e. 0.03 at June 4. Most probably, it helps discriminating crops at different growth stages (early or late), thanks to its sensitivity to the double-bounce scattering mechanism.

To conclude the analysis of the suitability of the PolInSAR parameters for crop classification, the confusion matrices considering the set of PolInSAR and PolSAR parameters have been evaluated and added to the supplementary material. The most consistently well classified crop is rice. The flooded ground provides this crop a very characteristic PolInSAR signature. When the ground is flooded, the SAR backscatter is very low, and when the plants start to grow, there is a dominant double-bounce ground contribution. Only when the rice is fully grown can be confused with other crops, e.g. wheat, since they then present a similar canopy structure. The next crop which is consistently well classified is cotton. The soft and fluffy fiber that grows in a boll provides it a unique canopy structure. On the other hand, crops such as beans, pea and chickpea, with shorter height and a more similar canopy structure can be confused to some extent.

VI. CONCLUSIONS

This letter evaluates the contribution of characteristic PolInSAR parameters, as described by the CoRe, for crop-type mapping by exploiting single-pass bistatic TanDEM-X data. The assessment is performed by means of a RF classifier. Even though the satellite observation period is constrained to three months (not the entire growth cycle), high classification scores of 89-94% are obtained at pixel and field level with the joint use of the most representative PolInSAR descriptors.

Results presented here corroborate the findings of previous studies exploiting X-band SAR data for crop classification, employing either purely PolSAR observables [5], [6], or in conjunction with interferometric descriptors [7], [8]. The accuracy achieved with the evaluated PolInSAR features, i.e. around 89-94% at pixel and field level, respectively, is of the order of that reached with polarimetric descriptors alone, e.g. OA of 93-95% with the backscattering power at the Pauli channels, but is does not exceed it. On the other hand, the TrCoh on its own has proven a key PolInSAR descriptor of the physical scene. With an OA of 75-87% at pixel and field level, it outperforms classification levels obtained at the linear and Pauli channels alone [8], i.e. OA = 70-86%, 68-88% with γ_{HH} and γ_{VV}; and 72-88%, 68-85% with γ_{P1} and γ_{P2}, respectively.

Overall, the PolInSAR parameters evaluated, and in particular the TrCoh, have proven suitable for crop classification. In addition, the accuracies reached slightly improve when classifying together with PolSAR parameters.

VII. ACKNOWLEDGEMENT

The German Aerospace Center (DLR) provided all the TanDEM-X data under project NTI-POLI6736. The reference data were provided by the Regional Government of Andalucía and the Spanish Agrarian Guarantee Fund (FEGA).

REFERENCES

[1] T. Fisette, P. Rollin, Z. Aly, L. Campbell, B. Daneshfar, P. Filyer, A. Smith, A. Davidson, J. Shang, and I. Jarvis, "AAFC annual crop inventory: Status and challenges," in *2nd Int. Conf. Agro-Geoinformatics Inf. Sustain. Agric. Agro-Geoinformatics*, pp. 270–274, 2013.

[2] G. Krieger, A. Moreira, H. Fiedler, I. Hajnsek, M. Werner, M. Younis, and M. Zink, "TanDEM-X: A Satellite Formation for High-Resolution SAR Interferometry," *IEEE Trans. Geosci. Remote Sens.*, vol. 45, pp. 3317–3341, Nov. 2007.

[3] S. R. Cloude and K. P. Papathanassiou, "Polarimetric SAR interferometry," *IEEE Trans. Geosci. Remote Sens.*, vol. 36, no. 5, pp. 1551–1565, 1998.

[4] J. M. Lopez-Sanchez, F. Vicente-Guijalba, E. Erten, M. Campos-Taberner, and F. J. Garcia-Haro, "Retrieval of vegetation height in rice fields using polarimetric SAR interferometry with TanDEM-X data," *Remote Sens. Environ.*, vol. 192, pp. 30–44, April 2017.

[5] R. Sonobe, "Parcel-Based Crop Classification Using Multi-Temporal TerraSAR-X Dual Polarimetric Data," *Remote Sens.*, vol. 11, no. 10, 2019.

[6] M. Busquier, J. M. Lopez-Sanchez, and D. Bargiel, "Added Value of Coherent Copolar Polarimetry at X-Band for Crop-Type Mapping," *IEEE Geosci. Remote Sens. Lett.*, vol. 17, no. 5, pp. 819–823, 2020.

[7] R. Sonobe, H. Tani, X. Wang, N. Kobayashi, and H. Shimamura, "Discrimination of crop types with TerraSAR-X-derived information," *Phys. Chem. Earth, Parts A/B/C*, vol. 83-84, pp. 2–13, Jan. 2015.

[8] M. Busquier, J. M. Lopez-Sanchez, A. Mestre-Quereda, E. Navarro, M. P. Gonzalez-Dugo, and L. Mateos, "Exploring TanDEM-X Interferometric Products for Crop-Type Mapping," *Remote Sens.*, vol. 12, no. 11, June 2020.

[9] T. Flynn, M. Tabb, and R. Carande, "Coherence region shape extraction for vegetation parameter estimation in polarimetric SAR interferometry," *IEEE Int. Geosci. Remote Sens. Symp.*, vol. 5, pp. 2596–2598, 2002.

[10] A. Marino, "Trace coherence: A new operator for polarimetric and interferometric SAR images," *IEEE Trans. Geosci. Remote Sens.*, vol. 55, no. 4, pp. 2326–2339, 2017.

[11] N. Romero-Puig, A. Marino, and J. M. Lopez-Sanchez, "Application of the Trace Coherence to HH-VV PolInSAR TanDEM-X Data for Vegetation Height Estimation," *IEEE Trans. Geosci. Remote Sens.*, vol. 60, 2022.

[12] S. R. Cloude, *Polarisation: Applications in Remote Sensing*. Oxford: Oxford University Press, 2009.

[13] F. D. Murnaghan, "On the Field of Values of a Square Matrix," *Proc. Natl. Acad. Sci. U. S. A.*, vol. 18, no. 3, pp. 246–248, 1932.

[14] L. Breiman, "Random forests," *Mach. Learn.*, vol. 45, no. 1, pp. 5–32, 2001.

Evaluation of PolInSAR Observables for Crop-Type Mapping Using Bistatic TanDEM-X Data

Noelia Romero-Puig, *Graduate Student Member, IEEE,* Juan M. Lopez-Sanchez, *Senior Member, IEEE*, Mario Busquier, *Student Member, IEEE*

Supplementary Material

I. Time Series of PolInSAR Observables

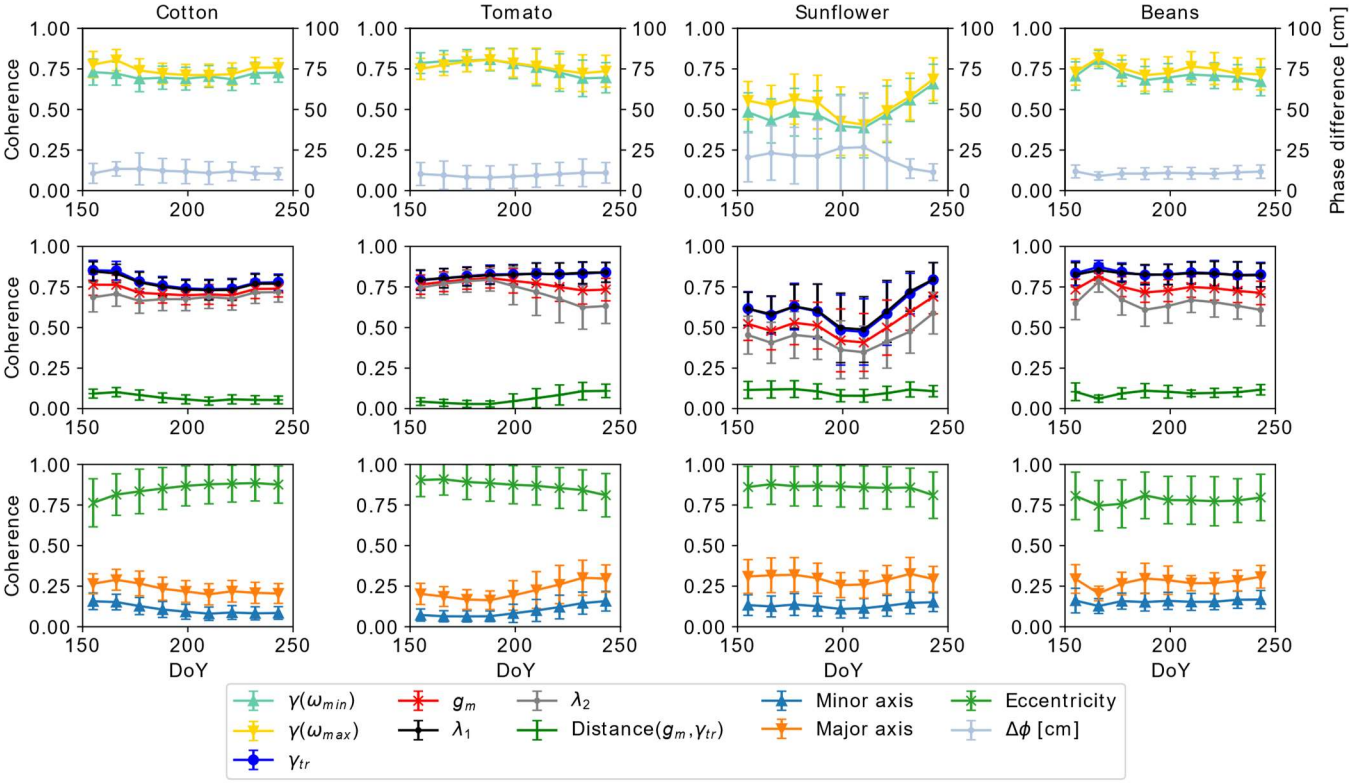

Fig. 1. Time series of PolInSAR observables, i.e. characteristic parameters of the CoRe, for 4 selected crop types: cotton, tomato, sunflower, beans. Average values of all available pixels for each crop type (including training and testing samples) are considered, and error bars denote ± standard deviation.

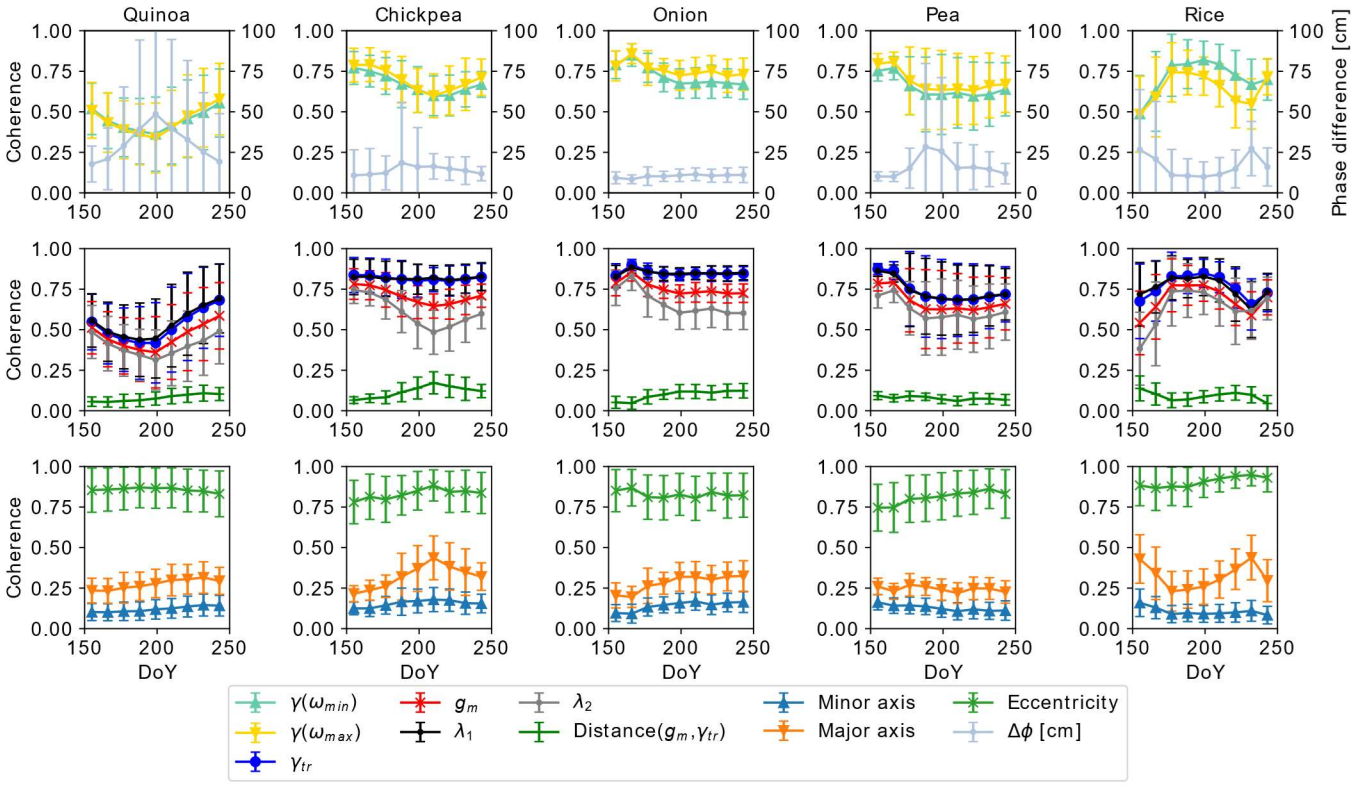

Fig. 2. Time series of PolInSAR observables, i.e. characteristic parameters of the CoRe, for 5 selected crop types: quinoa, chickpea, onion, pea, rice. Average values of all available pixels for each crop type (including training and testing samples) are considered, and error bars denote ± standard deviation.

II. Classification Importance of Input Features

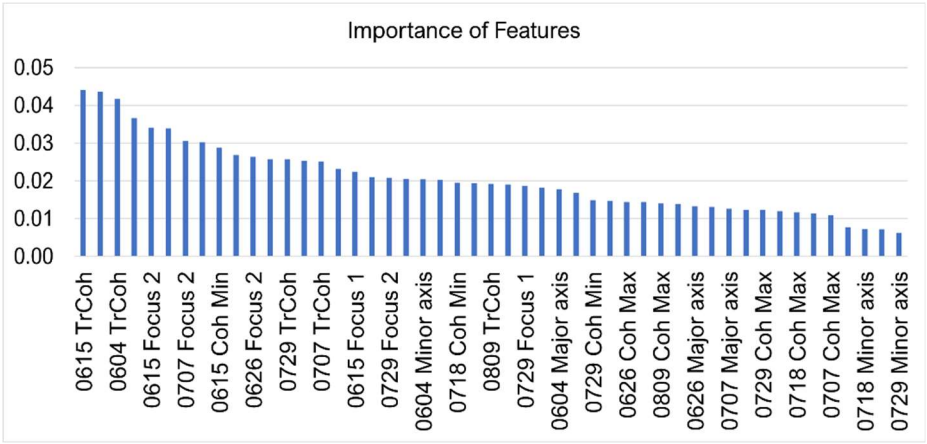

Fig. 3. Classification importance of the different input features provided by the RF algorithm. The feature set evaluated corresponds to **Set 1**, which includes: the TrCoh, the ellipse axes and foci and the coherence extrema.

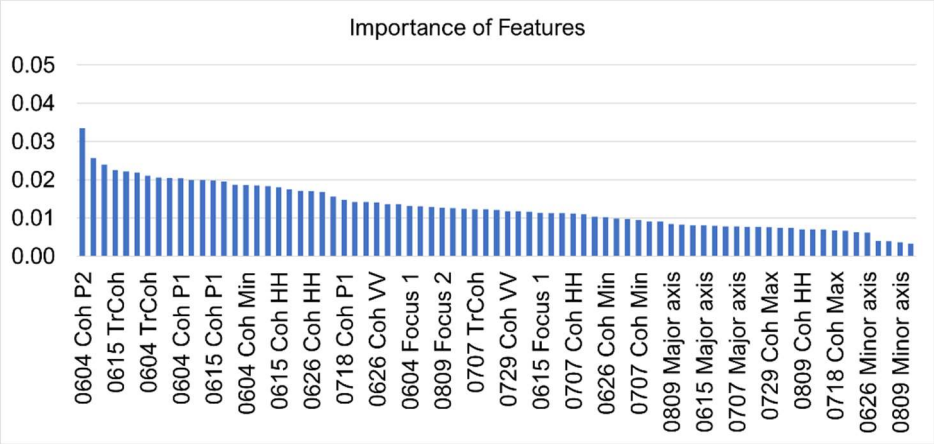

Fig. 4. Classification importance of the different input features provided by the RF algorithm. The feature set evaluated corresponds to all the PolInSAR features evaluated, including: the TrCoh, the ellipse axes and foci, the coherence extrema and the coherences at the linear and Pauli channels.

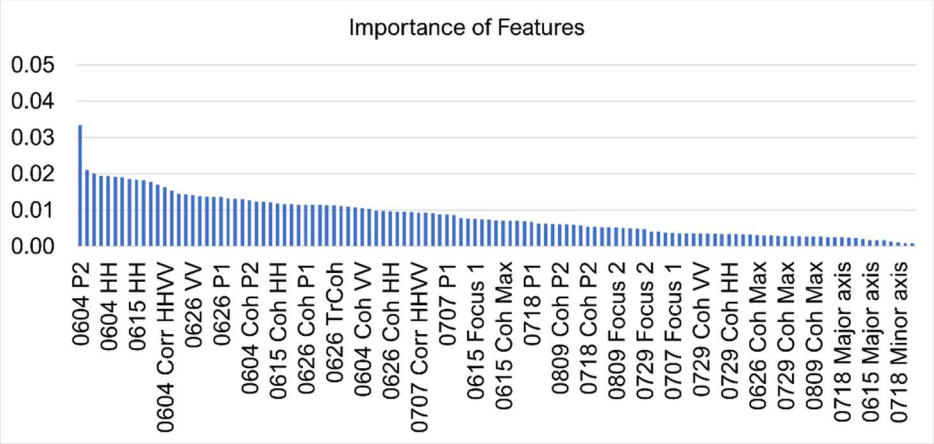

Fig. 5. Classification importance of the different input features provided by the RF algorithm. The feature set evaluated corresponds to all the PolSAR and PolInSAR features evaluated (see Section V. B).

III. Confusion Matrices

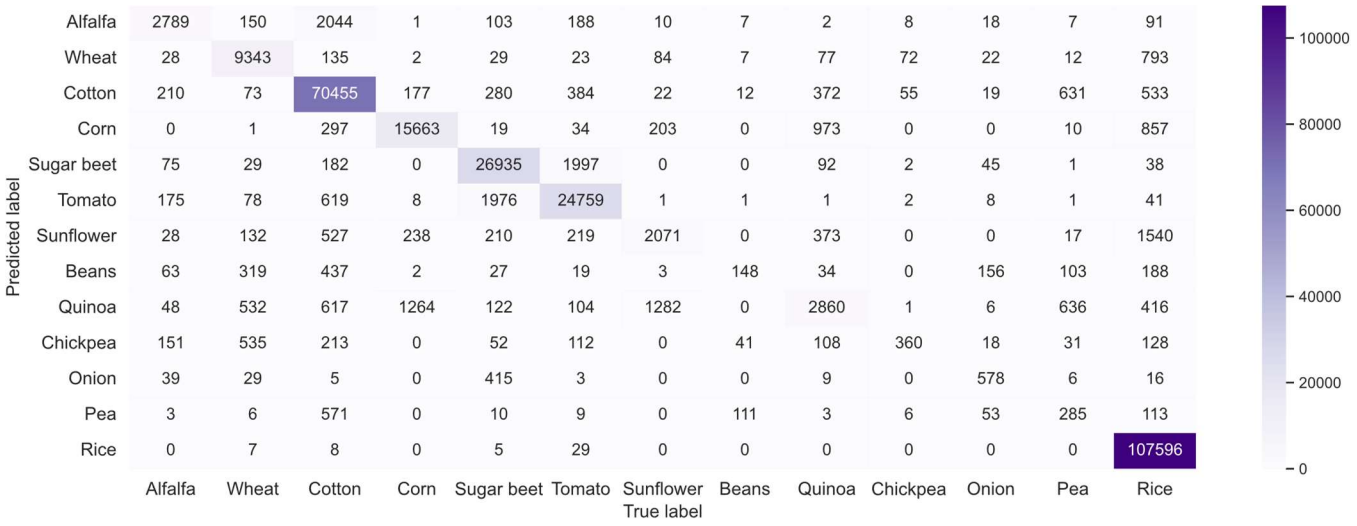

Fig. 6. Confusion matrix for the set of PolInSAR features (i.e. all those included in Table I) at pixel level.

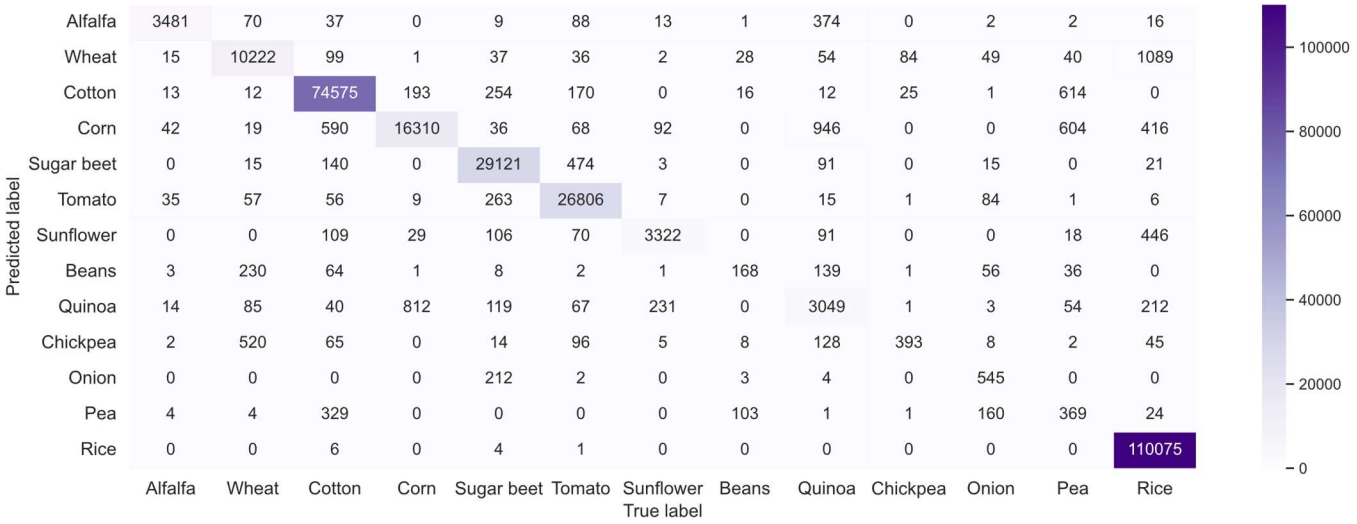

Fig. 7. Confusion matrix for the entire set PolInSAR and PolSAR features (i.e. those included in Table II except for the phase of the polarimetric correlation at the linear and Pauli channels, since they do not contribute with useful information to the classification) at pixel level.